

A GENUINELY MULTIDISCIPLINARY JOURNAL

CHEMPLUSCHEM

CENTERING ON CHEMISTRY

Accepted Article

Title: Reaction of Distonic Aryl and Alkyl Radical Cations with Amines: The Role of Charge and Spin Revealed by Mass Spectrometry, Kinetic Studies and DFT Calculations

Authors: Benjamin Andrikopoulos, Parvinder Sidhu, Bethany Taggart, Joses Nathanael, Richard O'Hair, and Uta Wille

This manuscript has been accepted after peer review and appears as an Accepted Article online prior to editing, proofing, and formal publication of the final Version of Record (VoR). This work is currently citable by using the Digital Object Identifier (DOI) given below. The VoR will be published online in Early View as soon as possible and may be different to this Accepted Article as a result of editing. Readers should obtain the VoR from the journal website shown below when it is published to ensure accuracy of information. The authors are responsible for the content of this Accepted Article.

To be cited as: *ChemPlusChem* 10.1002/cplu.201900706

Link to VoR: <http://dx.doi.org/10.1002/cplu.201900706>

WILEY-VCH

www.chempluschem.org

A Journal of



FULL PAPER

Reaction of Distonic Aryl and Alkyl Radical Cations with Amines: The Role of Charge and Spin Revealed by Mass Spectrometry, Kinetic Studies and DFT Calculations

Benjamin Andrikopoulos, Parvinder K. Sidhu, Bethany I. Taggart, Joses G. Nathanael, Richard A. J. O'Hair,* Uta Wille*[a]

Dedicated to Prof. Frances Separovic on the occasion of her 65th birthday and her retirement.

Abstract: Gas-phase reaction of the aromatic distonic radical cations 4-Pyr^{•+} and 3-Pyr^{•+} with amines led to formation of the corresponding amino pyridinium ions 4-Pyr⁺NR₂ and 3-Pyr⁺NR₂ through amine addition at the site of the radical, followed by homolytic β -fragmentation. The reaction efficiencies range from 66-100% for 4-Pyr^{•+} and 57-86% for 3-Pyr^{•+}, respectively, indicating practically collision-controlled processes in some cases. Computational studies revealed that the combination of positive charge and spin makes nucleophilic attack by the amine at the site of the radical barrierless and strongly exothermic by about $175 \pm 15 \text{ kJ mol}^{-1}$, thereby rendering 'conventional' radical pathways through hydrogen abstraction or addition onto π systems less important. Exemplary studies with 4-Pyr^{•+} showed that this reaction can be reproduced in solution. A similar addition/radical fragmentation sequence occurs also in the gas-phase reaction of amines with the aliphatic distonic radical cation Oxo^{•+}C⁺, showing that the observed charge-spin synergism is not limited to aromatic systems.

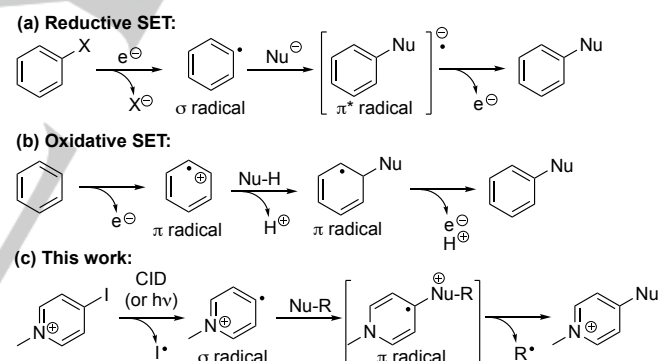
Introduction

Free radicals have found numerous applications in synthetic chemistry and are also involved in many biological systems, as well as intermediates in combustion and environmental transformation and degradation processes. Since the unpaired electron is considered as the most reactive site, it comes as no surprise that reactions involving radicals are commonly believed to proceed through radical pathways.

However, that this picture cannot be generalised is illustrated by several known reaction types where the unpaired electron seems to act as an 'observer' of non-radical process occurring in the same molecule. The Sandmeyer reaction is an example of a radical-nucleophilic aromatic substitution (S_{RN}1) that was discovered by Bunnett in 1970 (Scheme 1a)^[1] and involves a nucleophile (Nu) replacing an existing substituent X (most commonly a halogen atom) on the aromatic ring. The reaction is initiated by reductive single electron transfer (SET), which is

followed by dissociation to form a σ radical intermediate that is subsequently attacked by an N-, O- or C-nucleophile, such as sodium amide, an alkoxide or an enolate, respectively. During this addition the unpaired electron transitions into a π^* orbital, from where it is transferred onto another substrate to propagate the radical chain.

Removal of an electron from a π system, as shown in Scheme 1b for benzene as example, leads to a π radical cation, which can be trapped by either another radical through radical recombination (not shown) or by a nucleophile at the positive charge site.^[2] In the latter case the unpaired electron acts as a spectator during the bond-forming process. In the case of aromatic substrates, the sequence is usually terminated by a second oxidation and deprotonation that restores the aromatic π system.



Scheme 1. Examples for reactions of nucleophiles with radicals and radical ions.^[1,2]

Here we present a variation of this concept, which we discovered during an ongoing research project aimed at gaining a better mechanistic understanding of environmental radical polymer degradation. These processes are initiated at the gas/solid interface, which can be experimentally simulated by performing gas-phase studies in multi-stage mass spectrometers using the capability of ion traps to generate distonic radical ions, and then study their reactions with neutral compounds.^[3] The chemistry of reactant radical ions and charged reaction products can be directly monitored in a time resolved fashion to identify reactive intermediates associated with the formation of early degradation products,^[4] and to obtain kinetic data for individual reaction steps.

The distonic radical ion approach to study gas-phase radical reactions by mass spectrometry commonly considers the charge tag as innocent entity, which does not influence the mechanism

[a] Mr B. Andrikopoulos, Ms P. K. Sidhu, Ms B. I. Taggart, Dr. J. G. Nathanael, Prof. R. A. J. O'Hair, Prof. U. Wille
School of Chemistry, Bio21 Institute
The University of Melbourne
30 Flemington Road, Parkville, Victoria 3010, Australia
E-mail: rohair@unimelb.edu.au; uwille@unimelb.edu.au

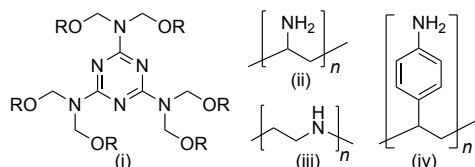
Supporting information for this article is given via a link at the end of the document.

FULL PAPER

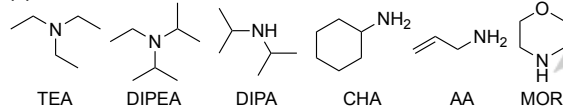
by which the radical reacts, compared to the neutral counterpart. Distonic radical ions have therefore been successfully employed to investigate radical reactions in many different areas, for example atmospheric chemistry,^[5] organic synthesis,^[6] and biological chemistry.^[7] Our previous studies, where we used distonic radical cations to explore the gas-phase chemistry of peroxy, alkoxy and alkyl radicals,^[6,8] enabled identification of several new reaction pathways that could contribute to polymer degradation under environmental conditions.^[9] However, Kenttämää *et al.* recently found that the radical reactivity of some distonic radical cations can be challenged by a competing nucleophilic reaction enabled by the positive charge.^[10]

Amines are prevalent structural moieties in polymers (Figure 1a), for example in melamine formaldehyde resins or melamine crosslinked polyesters (i), in polyamines, such as polyvinyl amine (ii), polyethylene imine (iii) and poly(aminostyrene) (iv).

(a) Amines in polymers:



(b) Model amines studied in this work:



(c) Distonic alkyl and aryl radical cations studied in this work:

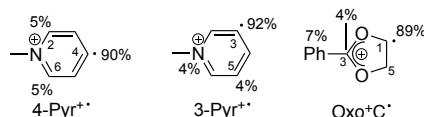


Figure 1. (a) Amine motifs in polymers and (b) model systems studied in this work; (c) spin densities in 4-Pyr^{+•}, 3-Pyr^{+•} and Oxo^{+•}C calculated with M062X/6-31+G*.

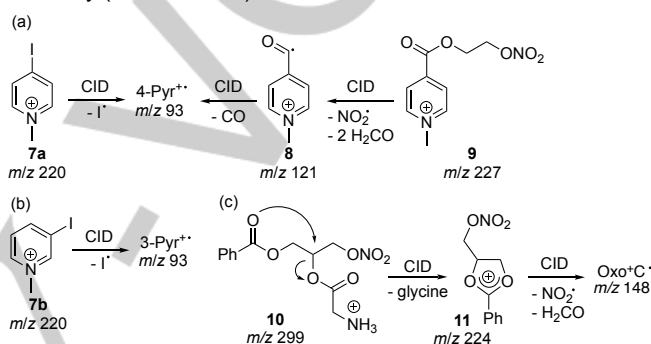
While hydrolytic degradation of melamine-containing polymers has been well studied,^[11] direct involvement of amine moieties in radical-mediated degradation has received considerably less attention. We have therefore explored the gas-phase reactions of the distonic aryl and alkyl radical cations 4-Pyr^{+•}, 3-Pyr^{+•} and Oxo^{+•}C with a series of primary, secondary and tertiary amines, e.g., triethyl amine (TEA), diisopropylethyl amine (DIPEA), diisopropyl amine (DIPA), cyclohexyl amine (CHA), allyl amine (AA) and morpholine (MOR) (Figure 1b,c), which represent simplified models for amine residues present in polymers with sufficient volatility to enable gas-phase studies in the ion trap mass spectrometer. Rapid nucleophilic addition of the amine to the distonic radical cation that is directed by the unpaired electron *in conjunction* with the charge is a key-finding (Scheme 1c), with 4-Pyr^{+•} reacting in a similar fashion also in solution. The experimental studies were augmented by DFT calculations to gain mechanistic understanding of these reactions, in particular to

define the interplay between charge and spin in these transformations.

Results and Discussion

1. Radical generation in the mass spectrometer

The distonic aryl and alkyl radical cations 4-Pyr^{+•}, 3-Pyr^{+•} and Oxo^{+•}C were generated *in situ* in the ion trap mass spectrometer (see Experimental Methods for details of the experimental set-up). The isomeric pyridinium radicals 3-Pyr^{+•} and 4-Pyr^{+•} (*m/z* 93) were obtained from the respective *N*-methyl iodo pyridines **7a** and **7b** through collision-induced dissociation (CID), as described previously (Scheme 2a,b).^[8a]



Scheme 2. Generation of the distonic radical cations 4-Pyr^{+•}, 3-Pyr^{+•} and Oxo^{+•}C in the mass spectrometer.

The pyridinium ester **9** was originally designed to access an O-centred alkoxy radical through CID of the labile O-NO₂ bond but rapid sequential loss of two H₂CO molecules led to the acyl radical **8** at *m/z* 121, which upon a second CID produced 4-Pyr^{+•} (Scheme 2a). The synthetic procedure and CID mass spectra for compound **9** are provided in the Supporting Information (SI, Figure S1). Comparison of the reactions of 4-Pyr^{+•} derived from precursors **7a** or **9** confirmed that its reactivity was independent of the generation method. We recently developed glycerol derivative **10** as precursor for Oxo^{+•}C (*m/z* 148), which is obtained through sequential CID *via* the cyclic tertiary carboxonium ion **11**,^[7d] followed by homolytic scission of the O-NO₂ bond and loss of formaldehyde (Scheme 2c).^[8b] According to DFT calculations (see below for details) the spin density in these distonic radical cations is predominantly (ca. 90%) located on the desired carbon atom (Figure 1c).

2. Gas-phase mass spectrometric studies

Reactions with Pyr^{+•}: Figure 2 shows the mass spectra of the ion-molecule reactions of 4-Pyr^{+•} with TEA (a), DIPEA (b), DIPA (c), and CHA (d), which were taken at reaction times where the signal intensity of 4-Pyr^{+•} had dropped to about 20% (120-240 ms). Product assignment was accomplished using computational studies (see section 3).

Interestingly, in the reaction with these amines the expected hydrogen atom abstraction (HAT) to give Pyr^{+•}H at *m/z* 94 was

FULL PAPER

only a very minor pathway.^[12] In the reaction with TEA the major product at m/z 165 could be assigned as the 4-diethylamino pyridinium ion **12a** resulting from formal addition of NEt_2^+ . The reaction with DIPEA led to a major product at m/z 179, which could be assigned as the ethyl isopropylamino pyridinium ion **13a**, suggesting a reaction through addition of the amine to the aromatic ring and loss of an isopropyl moiety. A product resulting from loss of an ethyl group (which would appear at m/z 193) was not formed. Similarly, the product at m/z 151 in the reaction with DIPA corresponds to the isopropyl amino pyridinium ion **14a**, resulting from formal addition of $\text{NH}i\text{Pr}^+$. In the reaction involving CHA, the product at m/z 109 could be assigned as the 4-amino pyridinium ion **15a**, which could be formed through formal addition of NH_2^+ . Products corresponding to addition of the amine to 4-Pyr^{•+} without elimination of an alkyl moiety were not detected in any of these reactions. Isolation of **12a** - **15a** in the ion trap showed no further reaction with the respective amine over several

seconds, suggesting closed-shell species. Fragmentation by CID only occurred only at very high energies, which further confirmed their stability. It should be noted that the products at m/z 100 in the reaction of TEA, at m/z 128 in the reaction of DIPEA, at m/z 100 and 102 in the reaction of DIPA, and at m/z 98 in the reaction of CHA could be assigned to protonated and/or oxidized amines, which were likely formed under the experimental conditions and not further investigated.^[13]

The reaction of 3-Pyr^{•+} with these four amines also led to formation of the respective isomeric 3-substituted products **12b** - **15b** (the site of amine substitution was elucidated computationally, see section 4). However, the HAT reaction to give Pyr^{•+}H appeared to be more favourable than in the reactions with 4-Pyr^{•+}. The mass spectra for the reaction of 3-Pyr^{•+} with TEA, DIPEA, DIPA and CHA are shown in Figures S2-S5.

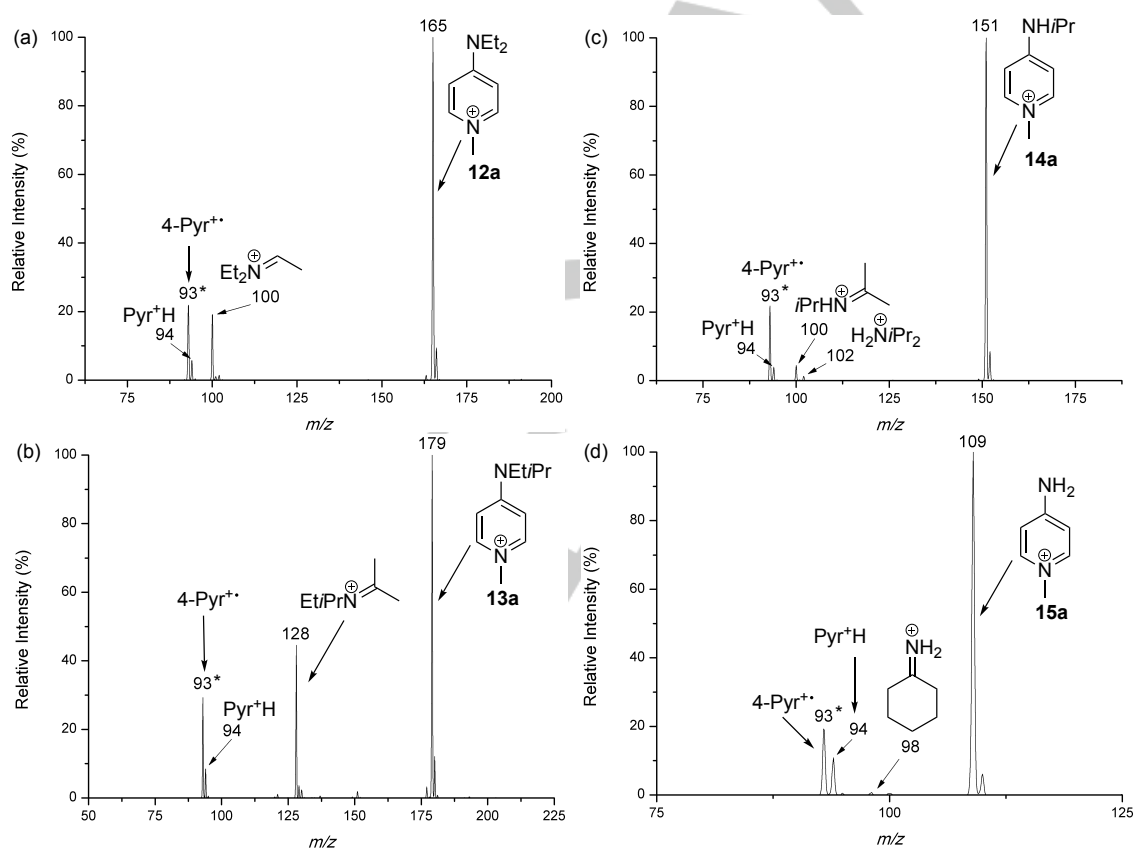


Figure 2. Mass spectra of the ion-molecule reactions of 4-Pyr^{•+} (m/z 93) with (a) TEA after 135 ms ($[\text{TEA}]$ ca. 1.2×10^{10} molecules cm^{-3}), (b) DIPEA after 240 ms ($[\text{DIPEA}]$ ca. 1.1×10^{10} molecules cm^{-3}), (c) DIPA after 120 ms ($[\text{DIPA}]$ ca. 1.2×10^{10} molecules cm^{-3}) and (d) CHA after 120 ms ($[\text{CHA}]$ ca. 1.2×10^{10} molecules cm^{-3}). The mass-selected precursor ion is indicated by an asterisk (*).

To compare the chemical reactivity of the isomeric Pyr^{•+}, we analysed the mass spectrometric yields obtained for the reaction with each amine at the same time point. Since mass discrimination could be excluded the peak area of each ionic species directly reflected their concentration. While the overall reactivity of both Pyr^{•+} with the amines is similar, compared with

4-Pyr^{•+} the reaction of 3-Pyr^{•+} gave a higher yield of the HAT product Pyr^{•+}H (m/z 94) at the expense of amine adduct formation, indicating a higher *radical* reactivity of the latter (Table S1).

To further explore this finding, we studied the reaction of AA, which could support radical pathways through both HAT (allylic C-H bonds) and addition (π -system). The mass spectra obtained

FULL PAPER

after 110 ms for the reaction of AA with 4-Pyr^{•+} and 3-Pyr^{•+} revealed clear differences between these two radical cations (Figure 3; the mass spectrometric yields at this time point are included in Table S1).

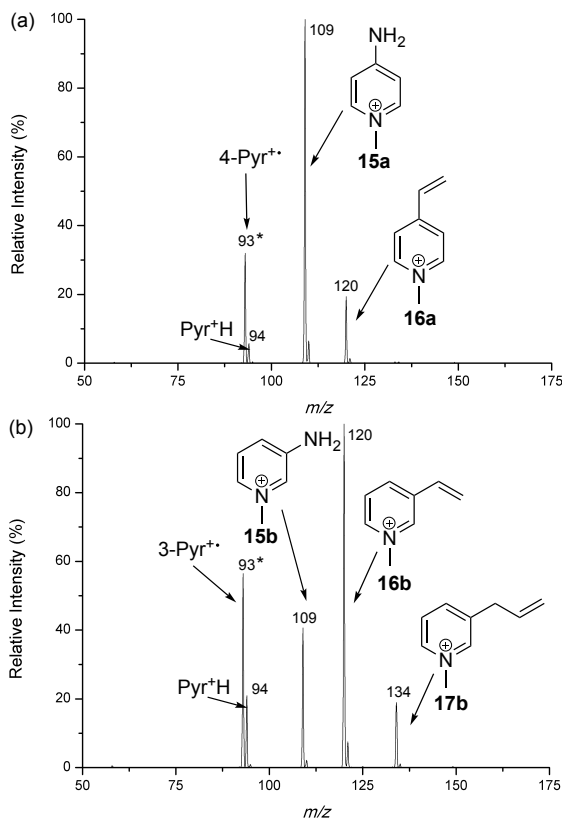


Figure 3. Mass spectra of the reaction of AA with (a) 4-Pyr^{•+} (m/z 93) and (b) 3-Pyr^{•+} (m/z 93) after 110 ms ([AA] ca. 1.2×10^{10} molecules cm^{-3}); the mass-selected precursor ion is indicated by an asterisk (*).

Thus, while the major product at m/z 109 in the reaction of 4-Pyr^{•+} could be assigned as the 4-amino pyridinium ion **15a** resulting from formal addition of the amine and loss of an allyl moiety (Figure 3a), the isomeric **15b** was obtained only as a minor product in the reaction of 3-Pyr^{•+}. Instead, the major product appeared at m/z 120, which could be assigned as the vinyl pyridinium ion **16b** (Figure 3b). In addition, small amounts of a product at m/z 134 also appeared, which could correspond to the allyl pyridinium ion **17b**. In the reaction of 4-Pyr^{•+}, on the other hand, the isomeric vinyl pyridinium **16a** was a minor product and only trace amounts of **17a** at m/z 134 were formed. Both products **16** and **17** indicate radical addition of Pyr^{•+} to the π -system in AA. Products from oxidation and/or protonation of AA could not be detected, because their masses were below the mass cut-off of the ion trap. Overall, formation of Pyr^{•+}H at m/z 94 through HAT was a minor reaction of both Pyr^{•+} but slightly more important for 3-Pyr^{•+} than for 4-Pyr^{•+}.^[14]

On the other hand, in the reaction of MOR with 3-Pyr^{•+} HAT and formation of Pyr^{•+}H was found as the major pathway. HAT also

occurred in the reaction with 4-Pyr^{•+}, but several unidentifiable products appeared at higher m/z values that suggest MOR addition, followed by fragmentation (see Figure S6).

Reactions with Oxo^{•+}C: Compared with both isomeric Pyr^{•+} the reaction of Oxo^{•+}C with amines was considerably slower. Figure 4 shows the mass spectrum of the reaction with TEA after 500 ms, where the signal intensity of unreacted Oxo^{•+}C was about 30%. The mass spectra of the reactions involving DIPEA and DIPA showed a similar outcome and are provided in Figure S7. While all reactions were characterised by significant amounts of protonation and/or oxidation side-products of the respective amines, none gave a product at m/z 149 corresponding to Oxo^{•+}CH, clearly excluding a pathway through HAT.

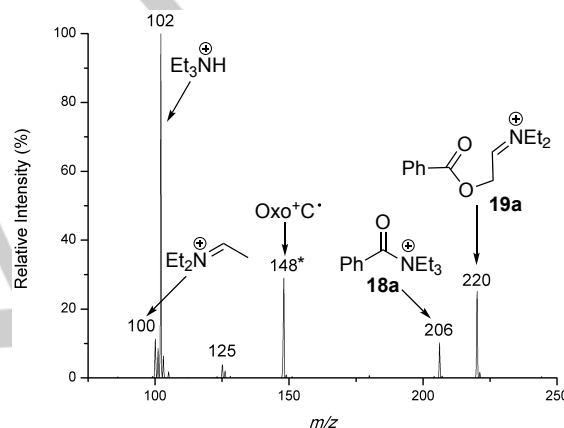
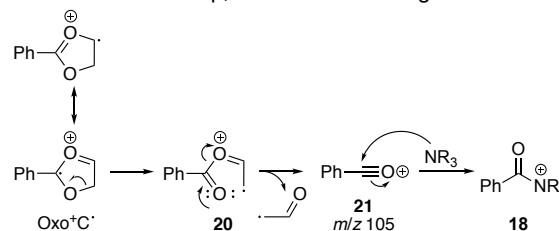


Figure 4. Mass spectrum of the reaction of Oxo^{•+}C (m/z 148) with TEA after 500 ms ([TEA] ca. 8.5×10^9 molecules cm^{-3}). The mass-selected precursor ion is indicated by an asterisk (*).

The adduct at m/z 220 formed in the reaction with TEA formally results from addition of NEt₂^{•+} to Oxo^{•+}C. Computational studies revealed the likely structure of the product as the open-chain iminium ion **19a** (see section 4). CID of **19a** showed fragmentation into an ion at m/z 105, which can be assigned as the phenylacylium ion PhC≡O⁺ (**21**). In addition, a product at m/z 206 was also formed, which was tentatively assigned as the acyl ammonium ion **18a**.^[15] We believe that the latter results from ring-opening of Oxo^{•+}C to **20**, followed by fragmentation into the acylium ion **21**,^[8b] which is subsequently trapped by the amine (Scheme 3). This assignment could be confirmed by CID on isolated **18a** in the ion trap, which revealed fragmentation into **21**.



Scheme 3. Proposed mechanism for formation of the acyl ammonium ions **18** in the reaction of Oxo^{•+}C with amines.

FULL PAPER

3. Kinetic studies of the gas-phase reaction of Pyr^{•+} with amines

Absolute rate coefficients for the consumption of Pyr^{•+} through reaction with TEA, DIPEA, DIPA, CHA and AA according to: Pyr^{•+} + amine → products, were obtained under quasi-thermal conditions by monitoring the decay of the Pyr^{•+} signal at *m/z* 93 ([M]^{•+}) as a function of reaction time under pseudo-first order conditions.^[8b] The rate coefficients for product formation, *i.e.*, Pyr^{•+}H, the adducts Pyr^{•+}-NR₂ as well as **16**, **17** and amine oxidation products were obtained from kinetic modelling of the experimental concentration-time profiles using the program Dynafit 4.^[16] Details are given in Experimental Methods.^[17] The rate data are compiled in Table 1. An exemplary concentration-time profile is shown in Figure S11, and the kinetic data for amine oxidation are compiled in Table S2. It should be noted that the concentration-time profiles for all products did not show any induction period, suggesting that they result from either a one-step reaction or from multistep processes, where intermediates are transformed into the products on faster timescales than can be resolved in the mass spectrometer. The mechanism will be discussed in section 4.

Table 1. Absolute second-order rate coefficients *k* for the reaction of 4-Pyr^{•+} and 3-Pyr^{•+} with amines at 298 K.^[a,b,c]

Amine	<i>k</i> × 10 ⁻¹⁰ (cm ³ molecule ⁻¹ s ⁻¹)			<i>k</i> _{Add} / <i>k</i> _{Rad} ^[d]	Efficiency ^[e]
	Pyr ^{•+} consumption	Pyr ^{•+} H formation	Pyr ^{•+} -NR ₂ formation		
TEA	8.9	0.8	9.1	11.4	70%
	<i>7.3</i>	<i>2.1</i>	<i>6.8</i>	<i>3.2</i>	<i>57%</i>
DIPEA	9.3	0.9	7.3	7.9	– ^[f]
	<i>8.0</i>	<i>1.4</i>	<i>4.2</i>	<i>3.0</i>	
DIPA	10	1.0	9.8	9.8	66%
	<i>8.1</i>	<i>2.3</i>	<i>8.4</i>	<i>3.7</i>	<i>58%</i>
CHA	15	2.7	15	5.6	100%
	<i>12</i>	<i>5.0</i>	<i>10</i>	<i>2.0</i>	<i>86%</i>
AA ^[g]	9.3	0.6	8.3	2.4	69%
	<i>8.2</i>	<i>0.7</i>	<i>3.3</i>	<i>0.4</i>	<i>61%</i>

[a] Data in first line for 4-Pyr^{•+}, in second line (in italics) for 3-Pyr^{•+}. [b] Rate coefficients for Pyr^{•+} consumption from pseudo-first order measurements; rate data for product formation were fitted using the Dynafit 4 program (see Experimental Methods). [c] Rate coefficients have an experimental error of 25%. [d] *k*_{Rad} = all radical processes (see text). [e] Determined from Pyr^{•+} decay rate using trajectory collision rate *k*_{ado} (× 10⁻⁹ cm³ molecule⁻¹ s⁻¹): TEA = 1.28, DIPA = 1.40, CHA = 1.40, AA = 1.35. [f] Not available (see text). [g] Rate coefficient (in cm³ molecule⁻¹ s⁻¹) for formation of **16a**: (2.8 ± 0.7) × 10⁻¹⁰, **16b**: (5.8 ± 1.5) × 10⁻¹⁰, **17b**: (1.0 ± 0.3) × 10⁻¹⁰.

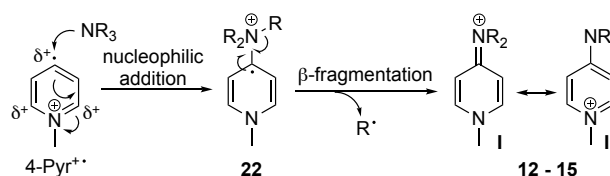
Overall, the reactions of both Pyr^{•+} with amines were very fast with the rate coefficients for the consumption of 4-Pyr^{•+} being about 20% higher than for 3-Pyr^{•+}. The reaction efficiencies, which were calculated from the trajectory collision rate, *k*_{ado}, derived from the average dipole orientation (ADO) theory^[18] for all amines (except for DIPEA for which polarizability data were not available from literature), range from 66-100% for 4-Pyr^{•+} and 57-86% for 3-Pyr^{•+}, respectively, indicating practically collision-controlled

reactions in some cases. Within error, the decay rate coefficients for Pyr^{•+} are similar to the sum of the rate coefficients for product formation, *e.g.*, Pyr^{•+}H, Pyr^{•+}-NR₂ and amine oxidation (see Table S2), confirming that no major pathway resulting in loss of the charge tag occurred, which would render the product undetectable by mass spectrometry.

Comparison of the rate coefficients *k*_{Add} for the formation of Pyr^{•+}-NR₂ with that for the 'conventional' radical pathways *k*_{Rad} through HAT or addition to π-systems (formation of Pyr^{•+}H, as well as **16a,b** and **17b** in the reaction involving AA) confirmed the differences in the chemical behaviour of both Pyr^{•+} observed in the product studies (section 2). For the reaction with the tertiary and secondary amines TEA, DIPEA and DIPA with 4-Pyr^{•+} a value for *k*_{Add}/*k*_{Rad} of 9.7 is obtained, whereas it is only 3.3 for 3-Pyr^{•+}, clearly showing the higher reactivity of 4-Pyr^{•+} for amine addition at the expense of conventional radical reactivity. This finding was confirmed by comparing *k*_{Add}/*k*_{Rad} for the reaction involving AA (where several sites are available to promote radical chemistry), which revealed a value of 2.4 for 4-Pyr^{•+} and only 0.4 for 3-Pyr^{•+}. For the reaction involving the less nucleophilic primary CHA, the ratio *k*_{Add}/*k*_{Rad} is about 50% smaller for both Pyr^{•+} compared with TEA, DIPEA and DIPA, respectively, which further supports the suggestion that formation of Pyr^{•+}-NR₂ involves nucleophilic amine addition to Pyr^{•+}.

4. Computational mechanistic studies

In recent gas-phase studies of isomeric dicationic pyridinium radical cations with amino acids Kenttämää *et al.* reported outcomes similar to those shown in Figures 2-4. They proposed that the reaction is initiated by nucleophilic addition of the amine to the pyridinium radical, where the efficiency of the transfer of the amino group was found to increase with the electron affinity of the radical cation; however, an 'active' role of the unpaired electron during the addition was not considered.^[10a,d,g] Thus, in the reaction with 4-Pyr^{•+} addition of NR₃ could occur at the radical site C-4, which should also be activated for nucleophilic attack, to form adduct **22**, which is followed by homolytic β-fragmentation to give the amino pyridinium ions **12-15** with release of R[•] (Scheme 4).^[19] In the reaction involving 3-Pyr^{•+}, where the sites of positive polarisation and unpaired electron do not coincide, NR₃ addition might occur at C-3 (radical site) as well as C-2 and C-4, which are activated by positive polarisation (not shown).



Scheme 4. Proposed mechanism for formation of the amino-substituted pyridinium ions **12** – **15** through non-radical addition of amines to Pyr^{•+}, followed by homolytic β-fragmentation (shown exemplarily for the reaction of 4-Pyr^{•+}).

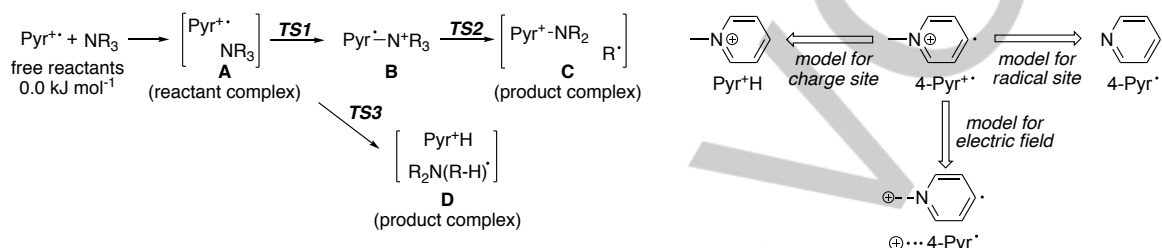
To better understand the interplay between charge and unpaired electron in these reactions, DFT calculations were performed at the M062X/6-31+G* level of theory,^[20a,21] which has been

FULL PAPER

previously shown to provide sufficiently accurate energies to identify the most likely reaction pathways.^[8b,22] The energies of the gas-phase calculations are given as enthalpies, as they best describe chemical reactivity under low-pressure bimolecular conditions,^[23] whereas for the reactions in solution (see section 5) free energies are considered. The Gaussian archive entries for all optimized stationary points, energies and imaginary frequencies for transition states are given in the SI.

Table 2 compiles the energies for the different reaction pathways of Pyr^{•+} with TEA, DIPEA and MOR. The reaction proceeds through formation of an initial ion-molecule association complex (reactant complex **A**) that is 40 - 60 kJ mol⁻¹ lower in energy than the free reactants, or 'entrance channel', which is defined as reference point and set to 0 kJ mol⁻¹. Pathways with energies above the entrance channel are too slow to occur on the timescale of the experiment.^[24]

Table 2. Gas-phase reaction of Pyr^{•+} with amines. M062X/6-31+G* enthalpies in kJ mol⁻¹, relative to the free reactants.



Entry	Pyr ^{•+}	amine	A	Reaction site in Pyr ^{•+}	TS1	B	TS2	C	TS3 ^[a]	D
1	4-Pyr ^{•+}	NEt ₃ (TEA)	-56.3	C-4	... ^[b]	-188.4	-104.7 ^[c]	-183.0 ^[c]	-28.9	-191.0
2	4-Pyr ^{•+}	NEtPr ₂ (DIPEA)	-51.9	C-4	... ^[b]	-157.9	-95.6 ^[c] -100.2 ^[e]	-193.2 ^[c] -208.0 ^[e]	... ^[d] -37.4 ^[f]	-- -215.1 ^[f]
3	4-Pyr ^{•+}	morpholine (MOR)	-46.8	C-4	... ^[b,g] -26.3 ^[h]	-157.6 ^[g] -45.3 ^[h]	--	--	-31.3 -19.5 ^[i]	-154.0 -123.1 ^[i]
4	3-Pyr ^{•+}	NEt ₃	-44.7	C-3 C-4	... ^[b] -41.1	-179.8 -50.4	-80.1 ^[c] --	-154.5 ^[c] --	-36.9	-198.5
5	Pyr ^{•+} H	NEt ₃	-43.3	C-4	-25.7	-28.1	--	--	--	--
6	4-Pyr [•]	NEt ₃	-14.6	C-4	32.7	16.4	--	--	--	--
7	⊕⋯⋯4-Pyr [•]	NEt ₃	-187.2 ^[k]	C-4	... ^[b]	-194.3	--	--	--	--

[a] HAT from N-CH₂. [b] No barrier (could not be located). [c] R[•] = Et[•]. [d] Not determined. [e] R[•] = *i*Pr[•]. [f] (R-H)[•] = *i*Pr[•]. [g] N addition. [h] O addition. [i] HAT from O-CH₂. [k] Geometry differed considerably from that of the other reactant complexes **A**.^[25]

A transition state **TS1** for the addition of the amine to the radical centre in 4-Pyr^{•+} (C-4) and in 3-Pyr^{•+} (C-3) could not be located,^[26] suggesting a barrierless step. Amine addition at C-4 in 3-Pyr^{•+} will be discussed below. Formation of the Pyr^{•+}-amine adducts **B** is strongly exothermic with 158 – 189 kJ mol⁻¹ (entries 1–4). The subsequent homolytic β-fragmentation via **TS2** is associated with a barrier of about 60–100 kJ mol⁻¹ and leads to the product association complex **C** in an essentially energy-neutral or in the case of 3-Pyr^{•+} slightly endothermic reaction. However, since **B**, **TS2** and **C** are energetically well below the entrance channel, the β-fragmentation should be very fast. These findings support the mass spectrometric data that adducts **B** could not be detected even at very short reaction times. Relief of steric strain in the case of DIPEA is likely responsible for the higher exothermicity of step

B → **C** (entry 2), where the calculations confirm the experimentally observed exclusive release of the more stable secondary radical *i*Pr[•] over the primary Et[•] (see Figure 2b).

Although HAT from the α-carbon atom in amines is thermodynamically highly favourable, this pathway is associated with a barrier (**TS3**) of 15–27 kJ mol⁻¹ for the reaction of 4-Pyr^{•+} with TEA and DIPEA, which cannot compete with the barrier-less formation of the amine adduct **B**. On the other hand, **TS3** is considerably lower for the reaction involving 3-Pyr^{•+} (27 vs 8 kJ mol⁻¹, entries 1 vs 4), which is in line with the experimentally observed higher radical reactivity of 3-Pyr^{•+}. In MOR the N-CH₂ moiety is the kinetically most favourable site for HAT, with **TS3** being about 15 kJ mol⁻¹ (entry 3). The computations predict also a barrierless addition of MOR to 4-Pyr^{•+} via the N atom. As

FULL PAPER

mentioned above and shown in the mass spectrum in Figure S6a, the signals at higher m/z values suggest that addition of MOR to 4-Pyr^{•+} occurred, but it was not possible to assign the various products that result from subsequent fragmentation of the 4-Pyr^{•+}-MOR adduct.

To evaluate the role of the radical site in 4-Pyr^{•+}, we calculated the addition of TEA to C-4 in the closed-shell Pyr^{•+}H (similar to a nucleophilic aromatic substitution, S_NAr). The data in entry 5 show that this addition is associated with a barrier of some 20 kJ mol⁻¹ and is endothermic. On the other hand, for the addition of TEA to C-4 in the neutral 4-Pyr[•] (similar to an S_{RN}1 mechanism; see Scheme 1a) both **TS1** and adduct **B** are located above the entrance channel, making this reaction too slow to occur under our experimental conditions (entry 6). These findings show that the unpaired electron in Pyr^{•+} in conjunction with the positive charge facilitate amine attack on the aromatic ring at the site of the unpaired electron. A similar accelerating effect on the amine addition was found, when the charge-causing methyl group in 4-Pyr^{•+} was replaced by a positive point charge (+1.0), i.e., ⊕⋯4-Pyr[•], to simulate an electric field (entry 8 vs 9 and 1).^[27]

Natural bond orbital (NBO) population analyses^[20b,28] revealed that in both 3- and 4-Pyr^{•+} the SOMO is submerged below the MOs of the aromatic π-electrons to become the fourth-highest energy molecular orbital (Figure 5a with 4-Pyr^{•+} as example, only the HOMO is shown, HOMO-1 and HOMO-2 on the remaining centres of the aromatic system are similar). The electron spin density plot shown exemplarily for 4-Pyr^{•+} confirms the sp² character of the SOMO on C-4, which is unrelated to the three higher lying occupied orbitals of the π system. On the other hand, the SOMO interacts with the σ* orbitals of neighbouring C-C bonds (LUMO+3 and LUMO+4), enabling delocalisation so that about 10% of the spin density in 4-Pyr^{•+} can be found on C-2 and C-6, and in 3-Pyr^{•+} on N and C-5, respectively (see also Figure 1).^[29,30]

Figure 5b shows the optimised geometry of adduct **B** in the reaction of 4-Pyr^{•+} with TEA. Only 5% of the spin density is located on the amine moiety, which is characterised by all four C-N bonds being slightly elongated compared with typical C-N single bonds (ca. 1.479 Å).^[31] The remaining 95% spin density is distributed over the pyridinium ring involving two p-shaped SOMOs at both C-4 and N (which are now also the two highest occupied MOs) and the π* orbitals of the connecting carbon framework (not shown), suggesting that adduct **B** could be described through the resonance forms **III** and **IV**. In the transition state (**TS2**) of the subsequent homolytic β-fragmentation, the SOMO (=HOMO) interacts with the σ* orbital (LUMO) of the breaking N-C bond. **TS2** occurs comparatively late on the potential energy surface with about 50% of the spin density on the leaving Et[•] fragment. The bond scission is accompanied by considerable contraction of the remaining N-Et bonds to practically single bond length, as well as of the N-Pyr bond, which at 1.383 Å is close to that of a partial C-N double bond (1.352 Å)^[31] and already resembles the product resonance structure **I** in Scheme 4.

As mentioned above, the addition of amines to 3-Pyr^{•+} could principally occur at the radical site C-3, as well as at C-2 and C-4, since both latter positions would be expected to be activated for nucleophilic attack. We will focus our discussion on the

reaction at C-3 and C-4. The calculations reveal that amine addition at C-3 is not only barrier-less but also thermodynamically clearly more favourable than at C-4, despite being the less electropositive site (Table 2, entry 4).

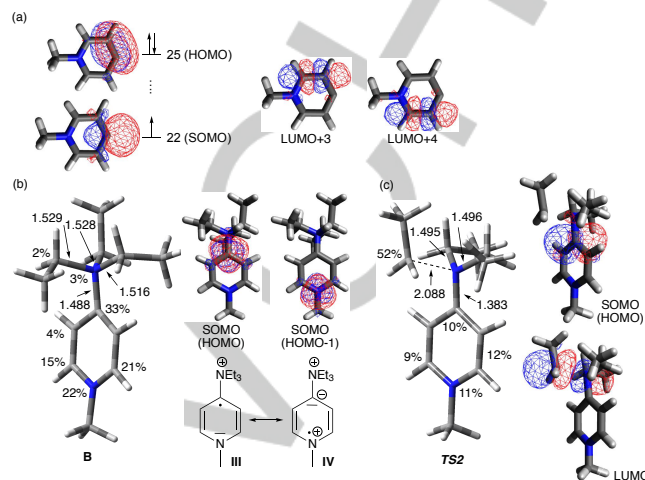


Figure 5. Reaction of 4-Pyr^{•+} with TEA. Geometries optimised with M062X/6-31+G*. (a) Electronic arrangement and MO configuration in 4-Pyr^{•+}; NBO population analysis with ωB97x/6-31+G*. (b) Geometry and MO configuration in adduct **B**; NBO population analysis with ωB97x/6-31+G*. (c) Geometry and MO configuration of transition state **TS2**; NBO analysis with M062X/6-31+G*. Bond lengths in Å, the percentage numbers are spin densities. The α electron spin density, highest doubly occupied molecular orbital (HOMO), singly occupied molecular orbital (SOMO) and selected lowest unoccupied molecular orbitals (LUMO) are indicated. The numbering of molecular orbitals is assigned in the order of increasing energy.

Figure 6a shows that the optimised geometries for **B** and **TS2** after initial amine addition at C-3 closely resemble those found for the addition at C-4 in 4-Pyr^{•+} with regards to both geometry and spin density. On the other hand, nucleophilic amine addition at C-4 in 3-Pyr^{•+} is associated with a small barrier (**TS1**) of 3 kJ mol⁻¹. Analysis of the orbitals revealed that the bond forming process involves interaction of the lone pair at N (in HOMO-1) with the LUMO at C-4 (MO not shown), without any contribution by the unpaired electron that is located in HOMO-4 (Figure 6b; HOMO, HOMO-2 and HOMO-3 are occupied by the six π electrons of the Pyr system). The adduct **B** is only slightly lower in energy than the reactant complex **A** and characterised by a long C-N bond of 1.619 Å and 90% spin density on C-3 (as in 3-Pyr^{•+}) and only 5% on the TEA moiety, clearly indicating that the unpaired electron is not involved in the amine addition at C-4.

The calculated energy profile for the reaction of Pyr^{•+} with AA revealed that the radical processes for 3-Pyr^{•+} through HAT and addition to the π system are lower in energy than for 4-Pyr^{•+}, confirming the experimentally found higher preference for 3-Pyr^{•+} to undergo 'conventional' radical chemistry. The data are presented in Scheme S1.

FULL PAPER

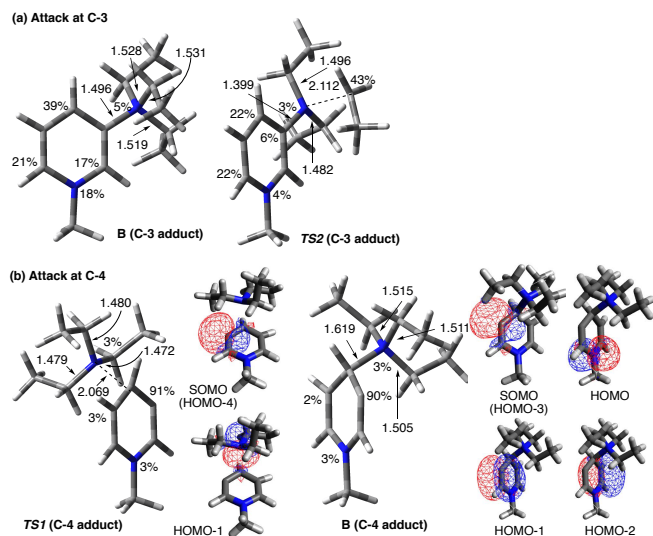


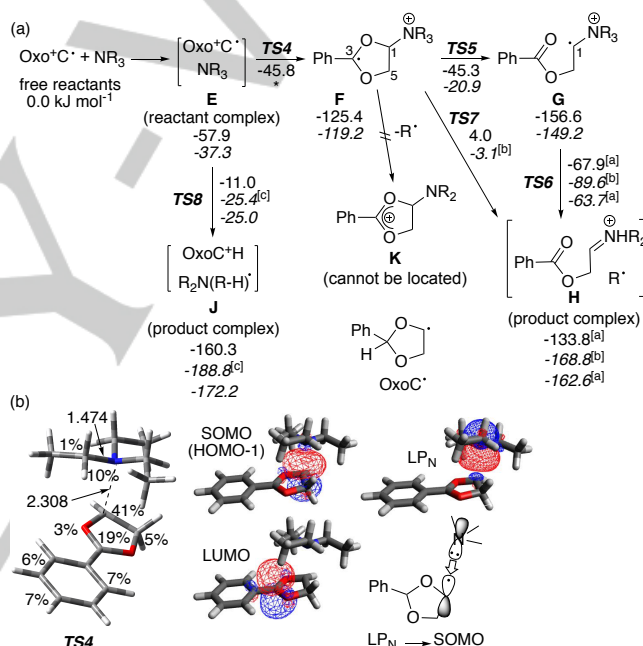
Figure 6. Reaction of 3-Pyr** with TEA. Geometries optimised with M062X/6-31+G*. (a) Adduct **B** and **TS2** during reaction at C-4. (b) **TS1** and adduct **B** during reaction at C-3. NBO population analysis of MO configuration analysed with M062X/6-31+G*. Bond lengths in Å, the percentage numbers are spin densities. The α electron spin density of relevant MOs is shown.

To conclude, upon amine addition to the radical site in either 3- or 4-Pyr** the SOMO transitions from an sp^2 orbital (σ radical) to a p orbital (π radical), enabling spin delocalisation over the Pyr ring that leads to stabilisation of adduct **B** by about 150-200 kJ mol^{-1} , compared to the reactions with the closed-shell (Pyr⁺H) or neutral (4-Pyr*) counterparts, respectively (Table 2, entry 1 vs 5 and 6). The unpaired electron is ejected *via* an alkyl radical in the subsequent homolytic β -fragmentation, leading to formation of the amino substituted pyridinium [Pyr-NR₂]⁺.

In contrast to Pyr**, amine addition to Oxo⁺C* occurs at a carbon centre that is not a part of an aromatic π system. Scheme 5a shows the calculated energies of the stationary points of the reaction of Oxo⁺C* with TEA and DIPEA. Amine addition to form the adduct **F** via **TS4** is kinetically considerably more favourable than HAT from the α -CH group in the amines via **TS8**, confirming the experimental finding that Oxo⁺CH (m/z 149) was not formed (see Figure 4). The geometry of **TS4** is shown in Scheme 5b for the reaction involving TEA, the geometries of all stationary points for this reaction are presented in Figure S19. **TS4** is characterised by a long C–N distance of 2.308 Å consistent with an early transition state. MO analysis revealed a strong interaction between the SOMO (= HOMO-1) and the LUMO on the tertiary carbon atom (C-3) of the dioxolane ring, enabling spin delocalisation. In the C–N bond forming process the SOMO accepts one electron of the lone pair at nitrogen, *i.e.*, LP_N → SOMO, leaving the non-participating electron on N (11% spin density). Formation of the adduct **F**, which has the SOMO centred on C-3, is strongly exothermic by about 120 kJ mol^{-1} . For comparison, the addition of TEA to the neutral radical OxoC* (see Scheme 5a) is predicted to be highly endothermic by ca 168 kJ mol^{-1} (data not shown), clearly revealing the role of the positive charge in Oxo⁺C* on the reaction energetics.

Attempts to compute a direct pathway from amine adduct **F** to the amino substituted dioxolanes **K** through homolytic β -fragmentation failed, but instead revealed the open-chain iminium complex **H**, which could be formed through a concerted ring-opening/ β -fragmentation.^[32] However, since the barrier **TS7** lies close to or even above the entrance channel, respectively, this pathway should be too slow to occur under our experimental conditions.

On the other hand, a stepwise mechanism consisting of radical ring-opening via **TS5** to yield the radical cation **G**, followed by homolytic β -fragmentation via **TS6** to yield **H** is highly feasible with all computed ground and transition states lying well below the entrance channel. It should be noted that for the reaction with DIPEA the predicted preferred radical scission of an N-*i*Pr bond over an N-Et bond in the fragmentation **G** → **H** is in agreement with the experimental findings (see Figure S7a).



Scheme 5. (a) M062X/6-31+G* enthalpies (in kJ mol^{-1}) of the stationary points for the various pathways in the reaction of Oxo⁺C* with TEA (top number) and DIPEA (bottom number in italics), relative to the free reactants. HAT pathway calculated for abstraction from the amine α -carbon. [a] R' = Et', [b] R' = *i*Pr', [c] HAT from secondary C-H in *i*Pr. ***TS4** for the addition of DIPEA could not be located, suggesting a barrier-less process. (b) Optimised geometry and MO configuration of **TS4** for the addition of TEA to Oxo⁺C*; NBO analysis with ω B97X/6-31+G*. Bond lengths in Å, the percentage numbers are spin densities. The α electron spin density, and selected molecular orbitals are indicated.

5. Reaction of 4-Pyr** with amines in solution

Since Kenttämäa *et al.* showed in previous work that distonic pyridine radical cations react with ethers, such as THF, in the condensed phase through both radical and non-radical pathways,^[10c,f] we explored whether the results from our mass spectrometric studies could also be reproduced in solution.^[33]

The experiments were performed by irradiating a solution of the radical precursor **7a** and the amine in acetonitrile in a Rayonet photoreactor with $\lambda = 350 \text{ nm}$ ^[10c] at 35°C for 24 hours. The

FULL PAPER

reaction mixture was analysed by direct injection ESI high-resolution mass spectrometry (HRMS, see Table S3), which provided confident assignment of the molecular formulae of the products. Generation of 4-Pyr^{•+} under these conditions was confirmed by irradiating a solution of **7a** in acetonitrile in the presence of two equivalents of the radical trap TEMPO. A product at m/z 249 was formed, which was confirmed by HRMS as the adduct 4-Pyr^{•+}-OTEMP (Figure S8).

The mass spectrum in Figure 7a shows that the reaction with TEA indeed led to formation of the adduct **12a** at m/z 165. No reaction occurred between **7a** and TEA in the absence of light under otherwise identical conditions (Figure S9), clearly excluding an S_NAr mechanism.

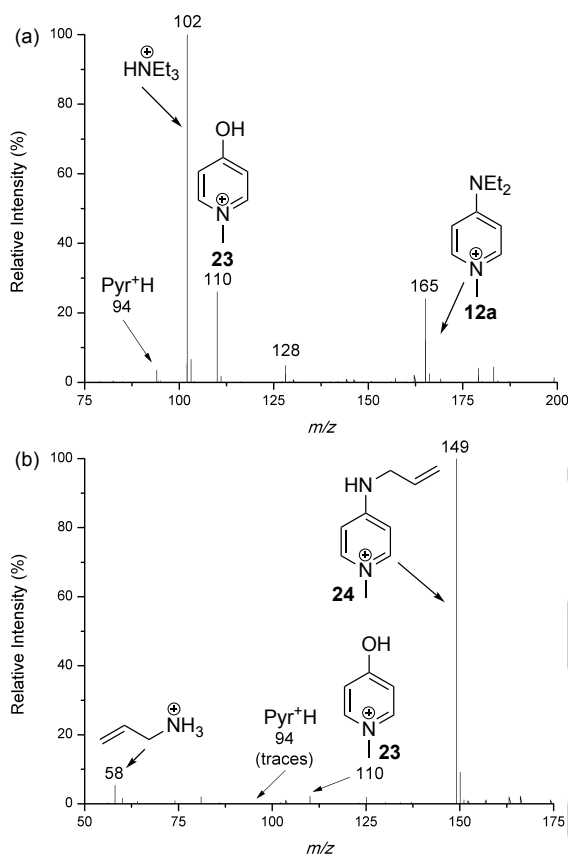
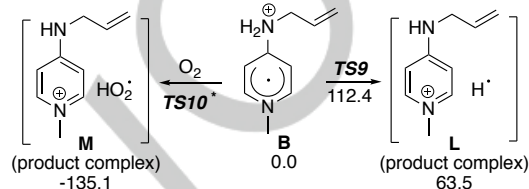


Figure 7. Mass spectra of the reaction of 4-Pyr^{•+} (**7a**, m/z 220, 0.086 mmol) in the Rayonet photoreactor ($\lambda = 350$ nm, 24 hrs, 35°C). (a) Reaction with TEA (1.79 mmol in 15 mL MeCN), (b) Reaction with AA (3.34 mmol in 15 mL MeCN). The HRMS data of the products are given in Table S3.

The major signal at m/z 102 could be assigned to protonated TEA that was present in excess. We also observed formation of a new product at m/z 110, which could be assigned as the hydroxy pyridinium **23** that could possibly result from reaction of 4-Pyr^{•+} with residual water in the solvent, which acts as the nucleophile. Product **12a** was isolated and its structure confirmed by ¹H NMR spectroscopy (Figure S20), providing further support for the proposed mechanism. Similar to the reactions in the gas phase, HAT and formation of Pyr^{•+}H was only a very minor pathway in the

reaction with amines in solution. Interestingly, the outcome of the reaction of 4-Pyr^{•+} with the primary amines AA and CHA in the condensed phase was different from that in the gas phase. In the reaction involving AA a product appeared at m/z 149 (Figure 7b), which could be assigned as the allylamine-substituted pyridinium **24**. Likewise, the product at m/z 191 formed in the reaction of 4-Pyr^{•+} with CHA corresponds to 4-cyclohexylamine pyridinium (**25**; shown in Figure S10a). Using the reaction with AA as example, the mechanism in Scheme 6 suggests that **24** result from the initially formed amine adduct **B** through hydrogen loss.



Scheme 6. Reaction of 4-Pyr^{•+} with AA in solution. M062X/6-31+G* free energies in acetonitrile (in kJ mol⁻¹) of the stationary points relative to the free reactants or relative to the adduct complex **B** – O₂ for the reaction involving O₂. *TS could not be located.

However, the calculated free energies for this homolytic scission in acetonitrile using the Conductor-like Polarizable Continuum Model (CPCM) model^[34] predict a barrier **TS9** of 112.4 kJ mol⁻¹ and an endothermicity of 63.5 kJ mol⁻¹, which seems to be unlikely to occur under the experimental conditions. We therefore propose that hydrogen abstraction proceeds with assistance of residual O₂ present in the solution. While a transition state for this abstraction could not be located, indicating a barrierless process, formation of the product complex **M** is strongly exothermic.^[35]

To explore whether the reaction is limited to amines, we performed the photolysis of **7a** in neat methanol and found formation of a product at m/z 124, which could be assigned as the 4-pyridinium methyl ether (**26**; shown in Figure S10b). When the reaction was performed in deuterated methanol, the mass shifted to m/z 127, confirming the proposed transfer of the OMe group onto 4-Pyr^{•+}. However, in contrast to the reactions with the amines, a large amount of unconsumed radical precursor **7a** was still present after 24 hours. Furthermore, when the reaction was performed with MeOH dissolved in acetonitrile, formation of 4-pyridinium methyl ether did not occur. These findings suggest that interception of the photogenerated tight radical pair [4-Pyr^{•+} I[•]] occurs more readily with the more nucleophilic amines allowing the reaction to be performed under dilute conditions using a solvent, whereas the lower nucleophilicity of MeOH requires partial separation of the ion pair for a reaction to occur, which can be achieved by performing the reaction in neat MeOH.^[36]

Conclusions

In this combined experimental and computational study, we have shown that the presence of a positive charge *in conjunction* with an unpaired electron considerably facilitates the nucleophilic addition of amines to pyridine. Using the isomeric distonic aryl

FULL PAPER

radical cations 4-Pyr^{•+} and 3-Pyr^{•+}, the reaction was found to occur through amine attack exclusively at the site of the unpaired electron, which is followed by homolytic β -fragmentation, where the unpaired electron is ejected *via* an alkyl radical to give the amino substituted pyridinium [Pyr-NR₂]⁺. This reaction is the dominant pathway, rendering 'conventional' radical reactions through HAT or addition to π systems of minor importance. However, in 3-Pyr^{•+}, where the site of spin and positive polarisation in the aromatic ring do not coincide, radical behaviour becomes slightly more important. The barrierless formation and particular stability of the amine adduct [Pyr-NR₃]^{•+}, compared with the endothermic formation of the closed-shell cationic adduct [Pyr-NR₃]⁺ through an S_NAr-type reaction, or the neutral radical adduct [Pyr-NR₃][•] through an S_{RN}1-type reaction, respectively, can be rationalised by the gain in energy resulting from transformation of the largely localised sp²-type SOMO in Pyr^{•+} into a p-type SOMO in [Pyr-NR₃]⁺ that enables delocalisation of the unpaired electron over the pyridine ring. Exemplary studies for 4-Pyr^{•+} revealed similar outcomes for the reaction with amines and even the weaker nucleophile methanol in solution.

A related amine addition/radical fragmentation sequence was also found in the reaction with the aliphatic distonic radical cation Oxo^{•+}C in the gas phase. These findings show that the synergistic effects caused by the combination of charge and spin are not limited to aromatic systems.

Experimental Methods

Mass Spectrometric Experiments. Gas-phase studies were conducted on a Thermo Scientific (Bremen, Germany) LTQ ESI mass spectrometer, modified to enable the introduction of volatile neutral reagents into the linear ion trap to perform ion-molecule reactions (IMRs). Briefly, a suitably volatile liquid reagent was injected at a rate of 5 – 20 $\mu\text{L hour}^{-1}$ directly into the helium line supplying helium bath gas to the linear ion trap. The helium line was heated and maintained at a temperature above the boiling point of the reagent, volatilising the liquid before it reached the ion trap. The pressure regulator controlling the flow of helium into the ion trap under normal operating conditions was bypassed, with the helium pressure controlled manually to maintain an ion gauge pressure that was the same as under normal operating conditions (0.69×10^{-5} Torr), which was confirmed by testing against the relatively slow ion-molecule reaction of Br[•] with CH₃I, as reported previously.^[37] Further details are given in refs.^[6,8,38] Ions undergoing ion-molecule reactions (IMRs) in the ion trap of the mass spectrometer are quasi thermalized to the temperature of the helium bath gas (298 K).^[38a] When performing IMRs, an ion of interest was isolated inside the ion trap, where it was allowed to react with the neutral. Each neutral compound used in the IMRs was purified prior to use *via* distillation, with purity checked by NMR.

Compound samples were prepared to 75–100 μM in methanol and were injected into the ESI source at a flow rate of 5 $\mu\text{L min}^{-1}$. The instrument was operated in positive ion mode, with the settings tuned to optimise the signal of the initial parent ion peak at the beginning of each data collection session. ESI source

conditions included needle potentials between 2.5–4.7 kV, a capillary temperature of 250°C, capillary voltages between 0.0–34.0, and tube lens voltages between 0.0–55.0 V. Ions of interest for MSⁿ experiments were isolated with a 2–5 m/z window. The CID parameter was selected so the parent ion being fragmented was reduced to ~15% abundance. Data were collected using three micro-scans and taking between 10–100 duplicate spectra.

Kinetic Studies. Absolute rate coefficients were determined from the peak areas in the mass spectra, which directly reflect the concentration of the respective ionic species in the ion trap. The rate coefficients for the consumption of Pyr^{•+} through reaction with the amines were obtained at 298 K by monitoring the decay of the Pyr^{•+} signal at m/z 93 ([M]^{•+}) as a function of reaction time under pseudo-first order conditions. Four to five different excess concentrations^[39] of the amine were used on time scales that allowed the peak intensity of Pyr^{•+} to decrease to ca. 20% and to build up time-resolved decay profiles (8–13 reaction times). The pseudo-first order rate coefficient k_{obs} was obtained from the slope of the plot $\ln[\text{Pyr}^{\bullet+}]$ vs. reaction time. The second-order rate coefficient k was determined by plotting k_{obs} vs. [amine], see Figures S12 and S13. The rate coefficients for product formation were obtained from kinetic modelling of the experimental concentration–time profiles using the program Dynafit 4.^[16] The pseudo-first order rate coefficients for product formation, k'_{obs} , were fitted for the HAT pathway: Pyr^{•+} + amine \rightarrow Pyr^{•+}H + [amine-H][•], at m/z 94, for the amine addition to Pyr^{•+}: Pyr^{•+} + amine \rightarrow Pyr^{•+}-NR₂, at m/z 165 (**12a/b**), m/z 179 (**13a/b**), m/z 151 (**14a/b**), m/z 109 (**15a/b**), m/z 120 (**16a/b**) and m/z 134 (**17b**) and for the amine oxidation Pyr^{•+} + amine \rightarrow amine-H^{•+} at m/z 100 (TEA and DIPA), m/z 128 (DIPEA) and m/z 98 (CHA). The second-order rate coefficient k for formation of each individual product was obtained from plotting k'_{obs} vs. [amine], which is shown in Figures S14 – S17 in the SI.

Acknowledgements

Support by the Australian Research Council (DP170100035 and DP180101187) and the Australian Government through provision of "Australian Government Research Training Program Scholarships" is gratefully acknowledged. The DFT calculations were performed on the Spartan High-Performance Computing (HPC) System hosted by Research Platform Services at the University of Melbourne.^[40] We thank the Bio21 Mass Spectrometry and Proteomics Facility for access to the Thermo Orbitrap Fusion Lumos mass spectrometer and Lars Goerigk for helpful discussions.

Keywords: DFT calculations • distonic ions • gas-phase chemistry • mass spectrometry • reaction mechanisms

- [1] J. F. Bunnett, J. K. Kim, *J. Am. Chem. Soc.* **1970**, *92*, 25, 7463–7464.
 [2] Selected examples: a) N. Holmberg-Douglas, D. A. Nicewicz, *Org. Lett.* **2019**, *21*, 7114; b) *Photochemistry* (Vol. 23), eds. D. Bryce-Smith, A. Gilbert, The Royal Society of Chemistry, 1992; c) J. G. Nathanael, L. F.

FULL PAPER

- Gamon, M. Cordes, P. R. Rablen, T. Bally, K. F. Fromm, B. Giese, U. Wille, *ChemBioChem* **2018**, *19*, 922.
- [3] K. M. Stirk, L. K. M. Kiminkinen, H. I. Kenttämäa, *Chem. Rev.* **1992**, *92*, 1649-1665.
- [4] Examples for the identification of early polymer degradation products: a) J. R. Lindsay Smith, E. Nagatomi, A. Stead, D. J. Waddington, S. D. Bévière, *J. Chem. Soc., Perkin Trans. 2* **2000**, 1193-1198; b) J. R. Lindsay Smith, E. Nagatomi, D. J. Waddington, *J. Chem. Soc., Perkin Trans. 2* **2000**, 2248-2258; c) J. R. Lindsay Smith, E. Nagatomi, A. Stead, D. J. Waddington, *J. Chem. Soc., Perkin Trans. 2* **2001**, 1527-1533.
- [5] Selected examples: a) A. K. Y. Lam, C. Li, G. N. Khairallah, B. B. Kirk, S. J. Blanksby, A. J. Trevitt, U. Wille, R. A. J. O'Hair, G. da Silva, *Phys. Chem. Chem. Phys.* **2012**, *14*, 2417-2426; b) C. Li, A. K. Lam, G. N. Khairallah, J. M. White, R. A. J. O'Hair, G. da Silva, *J. Am. Soc. Mass Spectrom.* **2013**, *24*, 493-501; c) A. T. Maccarone, B. B. Kirk, C. S. Hansen, T. M. Griffiths, S. Olsen, A. J. Trevitt, S. J. Blanksby, *J. Am. Chem. Soc.* **2013**, *135*, 9010-9014; d) G. da Silva, B. B. Kirk, C. Lloyd, A. J. Trevitt, S. J. Blanksby, *J. Phys. Chem. Lett.* **2012**, *3*, 805-811; e) B. B. Kirk, D. G. Harman, H. I. Kenttämäa, A. J. Trevitt, S. J. Blanksby, *Phys. Chem. Chem. Phys.* **2012**, *14*, 16719-16730.
- [6] a) C. H. Li, G. N. Khairallah, A. K. Y. Lam, R. A. J. O'Hair, B. B. Kirk, S. J. Blanksby, G. da Silva, U. Wille, *Chem. Asian J.* **2013**, *8*, 450-464; b) G. N. Khairallah, R. A. J. O'Hair, U. Wille, *J. Phys. Chem. A* **2014**, *118*, 3295-3306.
- [7] a) S. Osburn, B. Chan, V. Ryzhov, L. Radom, R. A. J. O'Hair, *J. Phys. Chem. A* **2016**, *120*, 8184-8189; b) S. Wee, A. Mortimer, D. Moran, A. Wright, C. K. Barlow, R. A. J. O'Hair, L. Radom, C. J. Easton, *Chem. Commun.* **2006**, 4233-4235; c) C. K. Barlow, A. Wright, C. J. Easton, R. A. J. O'Hair, *Org. Biomol. Chem.* **2011**, *9*, 3733-3745; d) R. A. J. O'Hair, *J. Mass Spectrom.* **2000**, *35*, 1377-1381.
- [8] a) B. Gervasoni, G. N. Khairallah, R. A. J. O'Hair, U. Wille, *Phys. Chem. Chem. Phys.* **2015**, *17*, 9212-9221; b) B. I. Taggart, R. A. J. O'Hair, U. Wille, *J. Phys. Chem. A* **2017**, *121*, 5290-5300.
- [9] The autoxidation mechanism used to rationalise radical degradation of all polymers, regardless of composition, has originally been proposed for the degradation of rubber, see: a) J. L. Bolland, *Proc. R. Soc. London Ser. A* **1946**, *186*, 218-236; b) J. L. Bolland, G. Gee, *Trans. Faraday Soc.* **1946**, *42*, 236-243; c) J. L. Bolland, P. ten Have, *Discuss. Faraday Soc.* **1947**, *2*, 252-260; d) L. Bateman, *Q. Rev. Chem. Soc.* **1954**, *8*, 147-167.
- [10] a) Y. Huang, L. Guler, J. Heidbrink, H. I. Kenttämäa, *J. Am. Chem. Soc.* **2005**, *127*, 3973-3978; b) A. Adeuya, J. M. Price, B. J. Jankiewicz, J. J. Nash, H. I. Kenttämäa, *J. Phys. Chem. A* **2009**, *113*, 13663-13674; c) F. Widaja, Z. Jin, J. J. Nash, H. I. Kenttämäa, *J. Am. Chem. Soc.* **2012**, *134*, 2085-2093; d) G. O. Pates, L. Guler, J. J. Nash, H. I. Kenttämäa, *J. Am. Chem. Soc.* **2011**, *133*, 9331-9342; e) B. J. Jankiewicz, J. Gao, J. N. Reece, N. R. Vinuesa, P. Narra, J. J. Nash, H. I. Kenttämäa, *J. Phys. Chem. A* **2012**, *116*, 3089-3093; f) F. Widaja, Z. Jin, J. J. Nash, H. I. Kenttämäa, *J. Am. Soc. Mass Spectrom.* **2013**, *24*, 469-480; g) P. E. Williams, B. J. Jankiewicz, L. Yang, H. I. Kenttämäa, *Chem. Rev.* **2013**, *113*, 6949-6985.
- [11] a) D. R. Bauer, *Appl. Polym. Sci.* **1982**, *27*, 3651-3662; b) C. Gao, S. Moya, H. Lichtenfeld, A. Casoli, H. Fiedler, E. Donath, H. Möhwald, *Macromol. Mater. Eng.* **2001**, *286*, 355-361.
- [12] In the gas phase, canonical radical cations of nucleobases and nucleosides react with related amines via a range of reactions including proton transfer, electron transfer, HAT, addition reactions and addition-fragmentation reactions: a) L. Feketeová, G. N. Khairallah, B. Chan, V. Steinmetz, P. Maître, L. Radom, R. A. J. O'Hair, *Chem. Commun.* **2013**, 49, 7343-7345; b) L. Feketeová, B. Chan, G. N. Khairallah, V. Steinmetz, P. Maître, L. Radom, R. A. J. O'Hair, *Phys. Chem. Chem. Phys.* **2015**, *17*, 25837-25844; c) L. Feketeová, B. Chan, G. N. Khairallah, V. Steinmetz, P. Maître, L. Radom, R. A. J. O'Hair, *J. Phys. Chem. Lett.* **2017**, *8*, 3159-3165.
- [13] Oxidation could be initiated by reaction of the amine, for example TEA, with the radical cation through electron transfer ($\text{Pyr}^{+\bullet} + \text{NEt}_3 \rightarrow \text{Pyr} + \text{N}^{+\bullet}\text{Et}_3$) or hydride transfer ($\text{Pyr}^{+\bullet} + \text{NEt}_3 \rightarrow \text{PyrH}^+ + \text{Et}_2\text{N}^+=\text{CHCH}_3$).
- [14] Isolation of the products **15-17** in the ion trap revealed no further reaction with the amine, and CID did not lead to any fragmentation, even at high collision energies, confirming their stability.
- [15] The gas-phase chemistry of related *N*-acylpyridinium ions has been examined: R. A. J. O'Hair, N. K. Androustopoulos, *Org. Lett.* **2000**, *2*, 2567-2570.
- [16] P. Kuzmic, *Anal. Biochem.* **1996**, *237*, 260-273.
- [17] Because of the significant side reactions of the amines, kinetic studies could not be performed for Oxo⁺C⁺.
- [18] a) K. F. Lim, *Quantum Chem. Program Exch. Bull.* **1994**, *14*, 3; b) T. Su, M. T. Bowers, *Int. J. Mass Spectrom. Ion Phys.* **1973**, *12*, 347-356. Dipole moments from: CRC Handbook of Chemistry and Physics, 82nd ed. [electronic resource], editor-in-chief D. R. Lide, CRC Press Boca Raton, Fla. 2001. Polarizabilities from: R. Bosque, J. Sales, *J. Chem. Inf. Comput. Sci.* **2002**, *42*, 1154-1163.
- [19] An alternative route to formation of the amine adducts **12 - 15** through an unprecedented homolytic substitution on the N atom of the amine by $\text{Pyr}^{+\bullet}$ can be excluded, since hypervalent ammonium radicals of type $\text{Me}_{(x=1-3)}\text{NH}_{(4-x)}^{\bullet}$ are unstable and only metastable as deuterated species: F. Turecek, *Top. Curr. Chem.* **2003**, *225*, 77-129 and cited references.
- [20] a) Gaussian 09, Revision B.01, M. J. Frisch, G. W. Trucks, H. B. Schlegel, G. E. Scuseria, M. A. Robb, J. R. Cheeseman, G. Scalmani, V. Barone, B. Mennucci, G. A. Petersson, H. Nakatsuji, M. Caricato, X. Li, H. P. Hratchian, A. F. Izmaylov, J. Bloino, G. Zheng, J. L. Sonnenberg, M. Hada, M. Ehara, K. Toyota, R. Fukuda, J. Hasegawa, M. Ishida, T. Nakajima, Y. Honda, O. Kitao, H. Nakai, T. Vreven, J. A. Montgomery, Jr., J. E. Peralta, F. Ogliaro, M. Bearpark, J. J. Heyd, E. Brothers, K. N. Kudin, V. N. Staroverov, R. Kobayashi, J. Normand, K. Raghavachari, A. Rendell, J. C. Burant, S. S. Iyengar, J. Tomasi, M. Cossi, N. Rega, J. M. Millam, M. Klene, J. E. Knox, J. B. Cross, V. Bakken, C. Adamo, J. Jaramillo, R. Gomperts, R. E. Stratmann, O. Yazyev, A. J. Austin, R. Cammi, C. Pomelli, J. W. Ochterski, R. L. Martin, K. Morokuma, V. G. Zakrzewski, G. A. Voth, P. Salvador, J. J. Dannenberg, S. Dapprich, A. D. Daniels, O. Farkas, J. B. Foresman, J. V. Ortiz, J. Cioslowski, D. J. Fox, Gaussian, Inc., Wallingford CT, 2009; b) Gaussian 16, Revision B.01, M. J. Frisch, G. W. Trucks, H. B. Schlegel, G. E. Scuseria, M. A. Robb, J. R. Cheeseman, G. Scalmani, V. Barone, G. A. Petersson, H. Nakatsuji, X. Li, M. Caricato, A. V. Marenich, J. Bloino, B. G. Janesko, R. Gomperts, B. Mennucci, H. P. Hratchian, J. V. Ortiz, A. F. Izmaylov, J. L. Sonnenberg, D. Williams-Young, F. Ding, F. Lipparini, F. Egidi, J. Goings, B. Peng, A. Petrone, T. Henderson, D. Ranasinghe, V. G. Zakrzewski, J. Gao, N. Rega, G. Zheng, W. Liang, M. Hada, M. Ehara, K. Toyota, R. Fukuda, J. Hasegawa, M. Ishida, T. Nakajima, Y. Honda, O. Kitao, H. Nakai, T. Vreven, K. Throssell, J. A. Montgomery, Jr., J. E. Peralta, F. Ogliaro, M. J. Bearpark, J. J. Heyd, E. N. Brothers, K. N. Kudin, V. N. Staroverov, T. A. Keith, R. Kobayashi, J. Normand, K. Raghavachari, A. P. Rendell, J. C. Burant, S. S. Iyengar, J. Tomasi, M. Cossi, J. M. Millam, M. Klene, C. Adamo, R. Cammi, J. W. Ochterski, R. L. Martin, K. Morokuma, O. Farkas, J. B. Foresman, and D. J. Fox, Gaussian, Inc., Wallingford CT, 2016.
- [21] Y. Zhao, D. G. Truhlar, *Theor. Chem. Acc.* **2008**, *120*, 215-241.
- [22] All ground and transition states were verified by vibrational frequency analysis at the same level of theory, and all identified transition states showed only one imaginary frequency. The spin expectation value, $\langle s^2 \rangle$, was very close to 0.75 after spin annihilation, except for the adduct complex **B - O₂** shown in Scheme 6, for which $\langle s^2 \rangle$ was 0.8.
- [23] P. D. Dau, P. B. Armentrout, M. C. Michelini, J. K. Gibson, *Phys. Chem. Chem. Phys.* **2016**, *18*, 7334-7340.
- [24] Because of the low pressure in the ion trap of the mass spectrometer, energy exchange through collisions with the surroundings can be excluded. Thus, the reactant complex has excess energy resulting from the internal and kinetic energy of the free reactants and the electrostatic

FULL PAPER

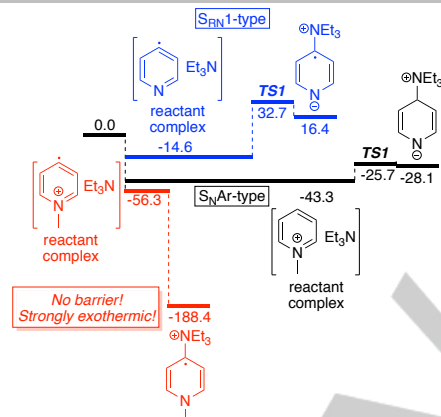
- energy that is released upon complex formation. Any subsequent reaction of the reactant complex is therefore only possible, if the activation barrier for this process is smaller or equal to the energy difference between the entrance channel and the association complex; see: a) C. H. DePuy, *J. Org. Chem.* **2002**, *67*, 2393-2401; b) M. Speranza, *Mass Spectrom. Rev.* **1992**, *11*, 73-117.
- [25] The optimised geometries of selected reactant complexes **A** are given in Figure S18. In complex [$\oplus\cdots$ 4-Pyr⁺-TEA] the N atom of TEA points towards the positive point charge, leading to significant stabilisation. It was not possible to locate a ground state geometry for [$\oplus\cdots$ 4-Pyr⁺-TEA] that was similar to the other reactant complexes.
- [26] The transition state for the addition of amines via N could only be located with UHF but not with DFT methods, such as BHandHLYP or M062X.
- [27] Selected examples: a) M. Klinska, L. M. Smith, G. Gryn'ova, M. G. Banwell, M. L. Coote, *Chem. Sci.* **2015**, *6*, 5623-5627; b) A. C. Aragonès, N. L. Haworth, N. Darwish, S. Ciampi, N. J. Bloomfield, G. G. Wallace, I. Diez-Perez, M. L. Coote, *Nature* **2016**, *531*, 88-91; c) R. Meir, H. Chen, W. Lai, S. Shaik, *ChemPhysChem* **2010**, *11*, 301-310; d) W. Lai, H. Chen, K.-B. Cho, S. Shaik, *J. Phys. Chem. Lett.* **2010**, *1*, 2082-2087; e) H. Hirao, H. Chen, M. A. Carvajal, Y. Wang, S. Shaik, *J. Am. Chem. Soc.* **2008**, *130*, 3319-3327; f) S. Shaik, S. P. de Visser, D. Kumar, *J. Am. Chem. Soc.* **2004**, *126*, 11746-11749; g) C. Geng, J. Li, T. Weiske, M. Schlangen, S. Shaik, H. Schwarz, *J. Am. Chem. Soc.* **2017**, *139*, 1684-1689; h) H. Schwarz, S. Shaik, J. Li, *J. Am. Chem. Soc.* **2017**, *139*, 17201-17212; i) L. Yue, N. Wang, S. Zhou, X. Sun, M. Schlangen, H. Schwarz, *Angew. Chem. Int. Ed.* **2018**, *57*, 14635-14639; and references therein.
- [28] NBO analyses performed with M062X/6-31+G* (large degree of Fock-exchange) and ω B97x/6-31+G* (range-separated hybrid; see: J.-D. Chai, M. Head-Gordon, *J. Chem. Phys.* **2008**, *128*, 084106) gave essentially identical results.
- [29] Population analyses confirmed that the SOMO is energetically below the MOs of the aromatic π system also in the σ -radicals Pyr⁺ and the phenyl radical Phe[•].
- [30] Analysis of Fractional Occupancy Density (FOD) plots (see: S. Grimme, A. Hansen, *Angew. Chem. Int. Ed.* **2015**, *12*, 12308) suggest that some intermediates where mixing of orbitals with excited states occurs, might require treatment by multireference methods. Unfortunately, such computations are too expensive for the comparably large systems studied in this work. Since the focus in this work is to obtain a qualitative understanding of the interactions between charge and spin in these reactions, single reference calculations provide a useful approximation.
- [31] CRC Handbook of Chemistry and Physics, 65th ed., (Eds. R. C. Weast, M. J. Astle, W. H. Beyer, CRC Press, Boca Raton, 1984.
- [32] The ground state of a cyclic amino substituted dioxolane **K** could not be located with UHF or DFT methods, clearly indicating that this framework is not stable.
- [33] For recent mechanism-based studies where gas-phase reactivity has been translated into new solution methods for organic synthesis, see: a) A. Noor, J. Li, G. N. Khairallah, Z. Li, H. Ghari, A. J. Canty, A. Ariafard, P. S. Donnelly, R. A. J O'Hair, *Chem. Commun.* **2017**, *53*, 3854-3857; b) Y. Yang, A. Noor, A. J. Canty, A. Ariafard, P. S. Donnelly, R. A. J O'Hair, *Organometallics* **2019**, *38*, 424-435.
- [34] Y. Takano, K. N. Houk, *J. Chem. Theory Comput.* **2005**, *1*, 70-77.
- [35] It should be noted that the same outcome was obtained when the reaction was performed in a degassed solution under Ar or in an O₂ stream, suggesting that very small amounts of O₂ are sufficient for the reaction to proceed. Further mechanistic studies on the termination step are clearly required.
- [36] Performing the reaction of 4-Pyr⁺I (**7a**) with amines or methanol in an Accelerated Weathering Tester (Q-LAB QUV-se, using UVA-340 fluorescent lamps) at 50°C for 6 hours led to increased amounts of substitution products, indicating that higher temperatures are beneficial for the reaction outcome.
- [37] a) S. Gronert, C. H. DePuy, v. M. Bierbaum, *J. Am. Chem. Soc.* **1991**, *113*, 4009; b) S. C. Brydon, Z. Ren, G. da Silva, S. F. Lim, G. N. Khairallah, M. J. Rathjen, J. M. White, R. A. J. O'Hair, *J. Phys. Chem. A* **2019**, *123*, 8200.
- [38] a) W. A. Donald, G. N. Khairallah, R. A. J. O'Hair, *J. Am. Soc. Mass Spectrom.* **2013**, *24*, 811-815; b) W. A. Donald, C. J. McKenzie, R. A. J. O'Hair *Angew. Chem. Int. Ed.* **2011**, *50*, 8379-8383.
- [39] T. Waters, R. A. J. O'Hair, A. G. Wedd, *J. Am. Chem. Soc.* **2003**, *125*, 3384.
- [40] L. Lafayette, G. Sauter, L. Vu, B. Meade, Spartan Performance and Flexibility: An HPC-Cloud Chimera. OpenStack Summit, Barcelona, October 27, 2016.

FULL PAPER

Entry for the Table of Contents

FULL PAPER

Working together! Nucleophilic addition of amines to aromatic distonic radical cations $\text{Pyr}^{+\bullet}$ is facilitated an interplay between spin and positive charge, which direct amine attack to the site of the unpaired electron. This synergism makes the reaction energetically more favourable than the related reactions in the absence of spin ($\text{S}_{\text{N}}\text{Ar}$ -type reaction) or charge ($\text{S}_{\text{RN}}1$ -type reaction).



Benjamin Andrikopoulos, Parvinder K. Sidhu, Bethany I. Taggart, Joses G. Nathanael, Richard A. J. O'Hair*, Uta Wille*

Page No. – Page No.

Reaction of Distonic Aryl and Alkyl Radical Cations with Amines: The Role of Charge and Spin Revealed by Mass Spectrometry, Kinetic Studies and DFT Calculations

Accepted Manuscript